



This is a repository copy of *Equatorial magnetosonic waves : do nonlinear interactions play a role in their evolution?*.

White Rose Research Online URL for this paper:  
<http://eprints.whiterose.ac.uk/156668/>

Version: Published Version

---

**Article:**

Walker, S.N. [orcid.org/0000-0002-4105-1547](https://orcid.org/0000-0002-4105-1547), Balikhin, M.A., Yearby, K.H. [orcid.org/0000-0002-7605-4393](https://orcid.org/0000-0002-7605-4393) et al. (1 more author) (2020) Equatorial magnetosonic waves : do nonlinear interactions play a role in their evolution? *Journal of Geophysical Research: Space Physics*, 125 (1). ISSN 2169-9380

<https://doi.org/10.1029/2019ja027572>

---

**Reuse**

This article is distributed under the terms of the Creative Commons Attribution (CC BY) licence. This licence allows you to distribute, remix, tweak, and build upon the work, even commercially, as long as you credit the authors for the original work. More information and the full terms of the licence here:  
<https://creativecommons.org/licenses/>

**Takedown**

If you consider content in White Rose Research Online to be in breach of UK law, please notify us by emailing [eprints@whiterose.ac.uk](mailto:eprints@whiterose.ac.uk) including the URL of the record and the reason for the withdrawal request.



[eprints@whiterose.ac.uk](mailto:eprints@whiterose.ac.uk)  
<https://eprints.whiterose.ac.uk/>



## RESEARCH ARTICLE

10.1029/2019JA027572

## Equatorial Magnetosonic Waves: Do Nonlinear Interactions Play a Role in Their Evolution?

S. N. Walker<sup>1</sup>, M. A. Balikhin<sup>1</sup>, K. H. Yearby<sup>1</sup>, and H. Aryan<sup>1</sup><sup>1</sup>Automatic Control and Systems Engineering, University of Sheffield, Sheffield, UK

## Key Points:

- The occurrence of nonlinear interactions during Equatorial Magnetosonic Wave periods is investigated
- The transfer function shows that nonlinear effects between the harmonics are negligible
- Bicoherence analysis confirms the absence of nonlinear interactions in the spacecraft measurements

## Correspondence to:

S. N. Walker,  
simon.walker@sheffield.ac.uk

## Citation:

Walker, S. N., Balikhin, M. A., Yearby, K. H., & Aryan, H. (2020). Equatorial magnetosonic waves: Do nonlinear interactions play a role in their evolution? *Journal of Geophysical Research: Space Physics*, 125, e2019JA027572. <https://doi.org/10.1029/2019JA027572>

Received 25 OCT 2019

Accepted 18 DEC 2019

Accepted article online 26 DEC 2019

**Abstract** The occurrence of nonlinear interactions between discrete wave frequencies has been shown to play a significant role in the propagation and evolution of some plasma wave modes. In this paper we take advantage of closely spaced Cluster measurements to investigate the possibility nonlinear interactions occurring between the discrete emissions that are observed in a region of Equatorial Magnetosonic Wave generation. Based on transfer function analysis, it is shown that the role of nonlinear interactions plays a negligible role in the wave evolution as the emissions propagate from one satellite to the other. A bicoherence analysis of the individual signals also fails to find the existence of nonlinear interactions in the evolution of equatorial magnetosonic waves.

**Plain Language Summary** In space plasmas, oscillations in the background electric and magnetic fields grow from energy sources associated with populations of plasma particles that are not in equilibrium. Once generated, these plasma waves may interact with the background plasma passing their energy back to the particles. In addition, waves at different frequencies may interact with each other, passing some of their energy to waves at a third frequency. These interactions may affect the evolution of these waves as they propagate in space. In this study, we examine a specific type of plasma wave, namely, equatorial magnetosonic waves, that exist as a set of harmonic frequencies related to the gyration of a proton in a magnetic field, looking for evidence of so called wave-wave interactions in a region. No evidence is found for such interactions. Thus, it appears that these waves will evolve by exchanging energy with plasma particles but not plasma waves.

## 1. Introduction

Equatorial magnetosonic waves (EMW) (or, simply, equatorial noise; Gurnett, 1976; Russell et al., 1970) are commonly observed in the terrestrial inner magnetosphere (Boardsen et al., 2016; Laakso et al., 1990; Perraut et al., 1982; Posch et al., 2015). They usually appear as a regularly spaced series of discrete emissions at frequencies corresponding to harmonics of the proton gyrofrequency in the region in which they were generated in the frequency range with an upper limit in the vicinity of the lower hybrid frequency. Outside of their generation region, the frequencies are unrelated to the local magnetic field magnitude (Santolik et al., 2016), and under certain conditions the frequency structure may appear washed out (Boardsen et al., 1992; Posch et al., 2015). In the vast majority of cases, EMWs appear continuous in time; however, instances of quasiperiodic EMW have also been observed (Boardsen et al., 2014; Fu et al., 2014; Němec et al., 2015). EMW propagate in a direction almost perpendicular to the external magnetic field, possess a low ellipticity, and their magnetic field vector is aligned with the external magnetic field. These characteristics essentially limit the longitudinal extent of these waves to around 10° of the magnetic equator, although observations at higher latitudes have been reported (Tsurutani et al., 2014; Zhima et al., 2015).

The generation of EMW has been strongly linked to the occurrence of proton ring distributions that exhibit a positive slope ( $\partial f / \partial v_{\perp} > 0$ ) (Balikhin et al., 2015; Horne et al., 2000; McClements, 1996; Meredith et al., 2008; Min & Liu, 2016; Perraut et al., 1982). Such distributions arise due to the injection of plasma sheet particles from the nightside and their subsequent energy dependant drift around the Earth (Lyons & Williams, 1984). For a sufficiently large gradient, linear dispersion theory leads to the generation of waves in the vicinity of harmonics of the proton gyrofrequency, that is, at intersections between the fast magnetosonic mode and harmonics of the various proton Bernstein modes provided that the ratio of the ring speed ( $V_r$ ) to Alfvén speed ( $V_A$ ) is large enough. Horne et al. (2000) suggested that the growth of waves at frequencies  $\omega > 30\Omega_p$  occurred when  $V_r > V_A$  while growth at frequencies  $\omega < 30\Omega_p$  was linked to  $V_r > 2V_A$ .

©2019. The Authors.

This is an open access article under the terms of the Creative Commons Attribution License, which permits use, distribution and reproduction in any medium, provided the original work is properly cited.

EMWs have been shown to interact with radiation belt electrons and ions through the Doppler shifted cyclotron resonance condition (1) (Horne et al., 2007).

$$\omega - n\Omega/\gamma - k_{\parallel}v_{\parallel} = 0, \quad (1)$$

where  $\omega$  is the angular wave frequency,  $n$  is the resonance number,  $\Omega$  is the particle gyrofrequency (either ions or electrons),  $k_{\parallel}$  is the parallel wave vector component, and  $v_{\parallel}$  the parallel electron velocity, resulting in both the energisation of particles and their loss through pitch angle scattering via the Landau resonance ( $n = 0$ ) since the cyclotron resonances occur at too high an energy to be significant (Horne et al., 2007).

As noted above, EMWs may be observed with either a discrete (Balikhin et al., 2015) or continuous (Boardsen et al., 1992) spectrum. In a pair of papers, Sun, Gao, Chen, et al. (2016) and Sun, Gao, Lu, et al. (2016) investigated the transition between these two states as a function of the input plasma parameters from the perspective of both linear theory and 1-D PIC simulations. Their results indicate that smaller values of either the proton to electron mass ratio, the ratio of the speed of light to the Alfvén velocity, or ratio of the ring velocity to the Alfvén velocity tended to result in a discrete spectrum. As these parameters increase, both the frequency and growth rate of the waves increased. When sufficiently high, a continuous, rather than discrete, spectrum results.

The results of another 1-D PIC simulations by Gao et al. (2018) showed that initial growth of EMWs, driven by an unstable proton ring distribution, occurred at harmonics in the range 9–12  $\Omega_p$ . Later in the simulation, emissions at lower harmonics were observed. These were attributed to the nonlinear interaction between the higher harmonics, as demonstrated by a bicoherence analysis. However, the maximum bicoherence value reported is small so any phase relation within the data may not be particularly significant.

In this study, we take advantage of data collected within the Cluster Inner Magnetospheric Campaign (2013) to investigate the occurrence of nonlinear processes in the evolution of EMW using a systems-based transfer function estimation methodology as well as bicoherence. This paper is structured as follows. Section 2 provides background on the Cluster Inner Magnetospheric Campaign and the data and methodology used in the analysis. The main results are presented and discussed in section 3.

## 2. Data and Methodology

At the beginning of July 2013 the Cluster mission embarked on its Inner Magnetospheric Campaign in which a “100 km formation” was initiated to investigate the role of plasma waves such as equatorial magnetosonic and chorus waves in the energization of electrons within the radiation belts. The data presented here were collected by the fluxgate (FGM) (Balogh et al., 1997) and search coil (STAFF) (Cornilleau-Wehrin et al., 1997) magnetometers aboard the Cluster 3 and 4 spacecraft (Escoubet et al., 1997) on 6 July 2013 between 18:30:00 and 19:00:00 UT. This period of data has previously been presented in studies by Balikhin et al. (2015) and Shklyar and Balikhin (2017).

During this period, the satellites traversed the inner magnetosphere at radial distance of 3.8–4.2  $R_E$ , local time 13:30–12:50, and a magnetic latitude of 1.9° to –2.3°, crossing the magnetic equator around 18:44 UT. Operating in science burst mode the data sets were sampled at 67 Hz (FGM) and 450 Hz (STAFF).

Figure 1 shows a spectrogram of the power spectral density of the equatorial magnetosonic emissions observed in the  $B_z$  (GSE) component of the magnetic field by the STAFF search coil magnetometers onboard Cluster 3 (Figure 1a) and Cluster 4 (Figure 1b). The maximum wave amplitudes measured for each harmonic are of the order 2–3 pT. Both spectrograms clearly show an instance of discrete, banded EMW occurring between the 20th and 30th harmonics of the proton gyrofrequency (indicated by the horizontal white lines). The actual frequencies of the emissions are observed to fall throughout the period, mirroring changes observed in the magnitude of the magnetic field. Thus, these observations took place in the generation region of the emissions. The time of the equatorial crossing is indicated by the vertical white line around 18:44 UT. Other (colored) vertical lines are the result of interference or spikes in the data.

## 3. Results

As mentioned in section 1 above, in this particular case, the EMWs were shown to be generated by a ring instability consisting of protons with energies of the order of 20–30 keV, and resulting in the generation of

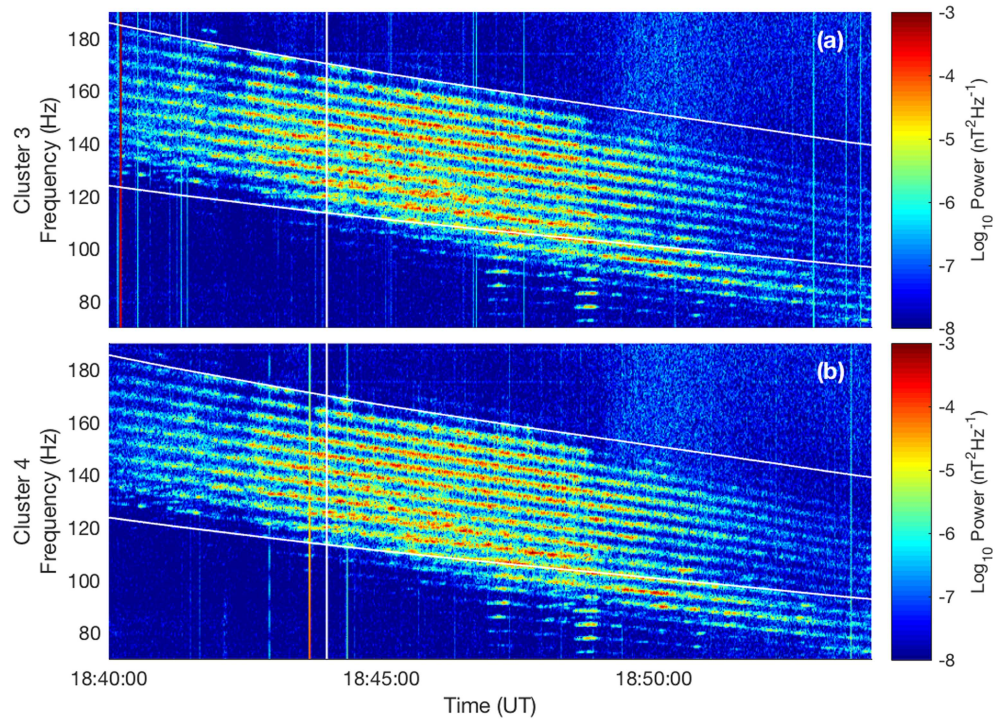


**Figure 1.** An overview of the magnetosonic wave emissions observed by the STAFF search coil instruments onboard Cluster Satellite 3 (panel a) and 4 (panel b) on 6 July 2013. The horizontal, sloping white lines represent the 20th and 30th harmonics of the proton gyrofrequency while the vertical white line indicated the approximate equatorial crossing time.

waves at frequencies corresponding to proton gyroharmonics in the range 16–32 (Balikhin et al., 2015). In the current study, the possibility of nonlinear interactions between these emissions is investigated.

Within a plasma, nonlinear interactions between waves at different frequencies are limited to either three-wave (decay instability) or four-wave interactions (modulational instability). Wave-wave coupling may only occur between waves that satisfy the certain conditions on both their frequencies ( $\omega$ ) and wave vectors ( $\vec{k}$ ) (Sagdeev & Galeev, 1969). In the case of a three-wave interaction, the waves must satisfy the resonance conditions

$$\omega = \omega_1 \pm \omega_2, \quad (2)$$

$$\vec{k} = \vec{k}_1 \pm \vec{k}_2. \quad (3)$$

The latter condition also implies that the phases ( $\phi$ ) of the waves are also related such that  $\phi_1 + \phi_2 - \phi = const.$

In this study two methods are employed to look for the possible occurrence of nonlinear wave-wave interactions, namely, the transfer function and bicoherence. Transfer functions are used to model the evolution of waves as they propagate between two points. In essence the measurements can be considered to be the input and output of a black box representation of the plasma between them, that is, a causal system. Knowledge of the transfer function may yield a deeper insight into the underlying physics of the system.

The dynamics of a stationary wavefield, sampled at two spatial locations, may be considered as an input-output system for which the relationship between  $y(t)$  (the output) and  $u(t)$  (the input) may be expressed in terms of a linear combination of the lagged input signals, using a nonlinear, continuous function  $F$  as shown in (4):

$$y(x, t) = F(y(x, t-1), y(x, t-2), \dots, u(x, t), u(x, t-1), u(x, t-2), \dots, \epsilon), \quad (4)$$

where  $y$  represents the output on the system measured at various times ( $t-1$ ), ( $t-2$ ), and so forth;  $u$  its input; and  $\epsilon$  is an error term. The function  $F$  may be expanded in terms of a Volterra series that consists of a set of

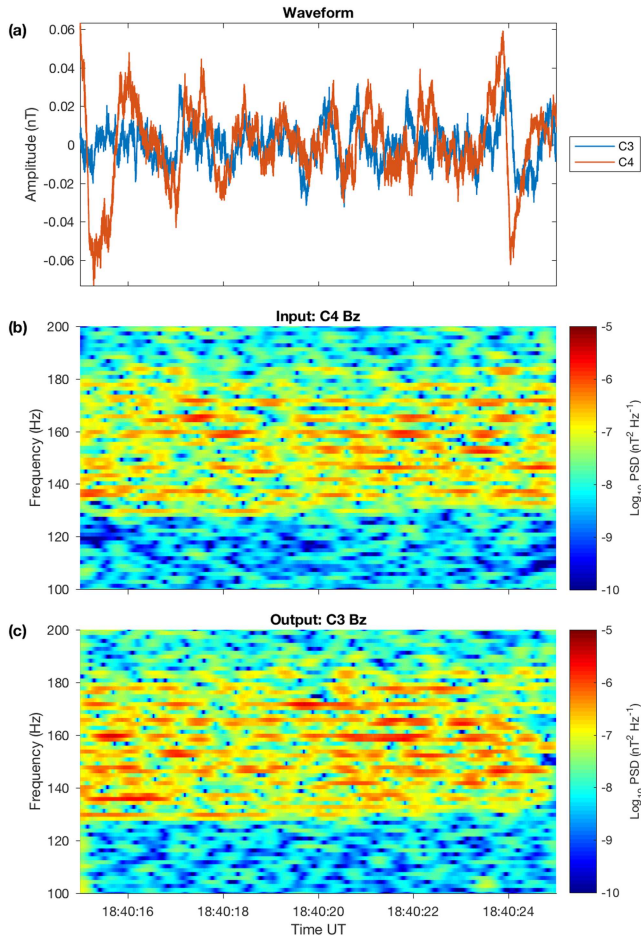


**Figure 2.** Waveform and spectra of data used in the analysis. Panel a shows the 10-s snapshot of the  $B_z$  magnetic field component measured by Cluster 3 (blue) and 4 (red). Panels b and c show wavelet spectrograms of the Cluster 3 and 4 waveforms in the frequency range 100–200 Hz.

kernels  $h$  that are directly related to the linear and higher-order spectral processes (5) (Billings, 2013).

$$y(t) = h_0 + \sum_{m_1=0}^M h_1(m_1)u(t-m_1) + \sum_{m_1=0}^M \sum_{m_2=0}^M h_2(m_1, m_2)u(m_1)u(m_2) + \dots \quad (5)$$

In the time domain, the terms  $h_l$  correspond to the  $l$ th-order impulse response functions of the system while the frequency domain equivalents are the  $l$ th-order transfer functions.

The use of real data (i.e., finite, noisy measurements) can affect the robustness of estimations of the Volterra kernels, even if we assume a Gaussian distribution. To increase the robustness of our estimations, we adopt a more generalized procedure based on the methodology developed by Ritz and Powers (1986) and further improved upon by Kim and Powers (1988) and Nam and Powers (1994). In the frequency domain methodology developed by these authors, the output signal  $Y(\omega)$  may be expressed as a function of the input signal  $U(\omega)$  and the linear  $L_\omega$ , quadratic  $Q_\omega$ , and higher-order spectral transfer functions as shown in (6).

$$Y_\omega = L_\omega U_\omega + \frac{1}{2} \sum_{\omega=\omega_1+\omega_2} Q_{\omega_1\omega_2}^\omega U_{\omega_1} U_{\omega_2} + \dots \quad (6)$$

To solve (6), it is necessary to convert the time domain measurements into a frequency domain representation. There are two commonly used methods to perform this task, the Fourier transform or the wavelet transform. The main difference between the two is the trade-off between the low time-resolution, high-frequency resolution results using the Fourier transform and the high time-resolution, lower-frequency resolution provided by the wavelet transform. In this study transfer to the frequency domain representation is performed using a wavelet transform since it was felt that this proved the best compromise between frequency and time resolutions.

The continuous wavelet transform is defined as

$$y(a, \tau) = \int y(t) \frac{1}{\sqrt{a}} h\left(\frac{t-\tau}{a}\right) dt, \quad (7)$$

where  $a$  is the scale of the analyzing wavelet  $h(t)$ . In order to optimize the time/frequency resolution trade-off, as well as to preserve phase information, the Gaussian or Morlet analyzing wavelet (8) was employed:

$$h(t) = \frac{1}{\pi^{1/4} \sigma^{1/2}} \exp(2\pi i t) \exp(-t^2/2\sigma^2), \quad (8)$$

where the scale and angular frequency are related by  $\omega = 2\pi/a$ . The parameter  $\sigma$  controls the width of the wavelet. The frequency resolution of the Morlet wavelet is defined as  $\Delta\omega/\omega = 1/4\sigma$ , and so the width of the wavelet may be adjusted to ensure there is no or minimal spectral overlap between adjacent channels. If  $\sigma$  is kept constant, the bandwidth of the wavelet transform becomes increasingly wider as the central frequency increases and structure in the data may be wiped out. The use of a wavelet transform also enables statistically robust results to be obtained based on the analysis of shorter time series.

As can clearly be seen from Figure 1, the frequencies of the proton gyroharmonics decrease throughout the period of data being studied. As a result, the duration of the period used in the following analysis is limited 10 s, between 18:40:15 and 18:40:25 UT, during which the frequency spectra show no significant change in frequency.

Figure 2 shows the 10-s snap shot of data used in the current study. Figure 2a shows waveform of the GSE  $B_z$  component measured by the STAFF search coil magnetometers onboard Cluster 3 (blue) and Cluster 4 (red). These waveforms have been detrended by removing their mean values. Typical amplitudes are of the

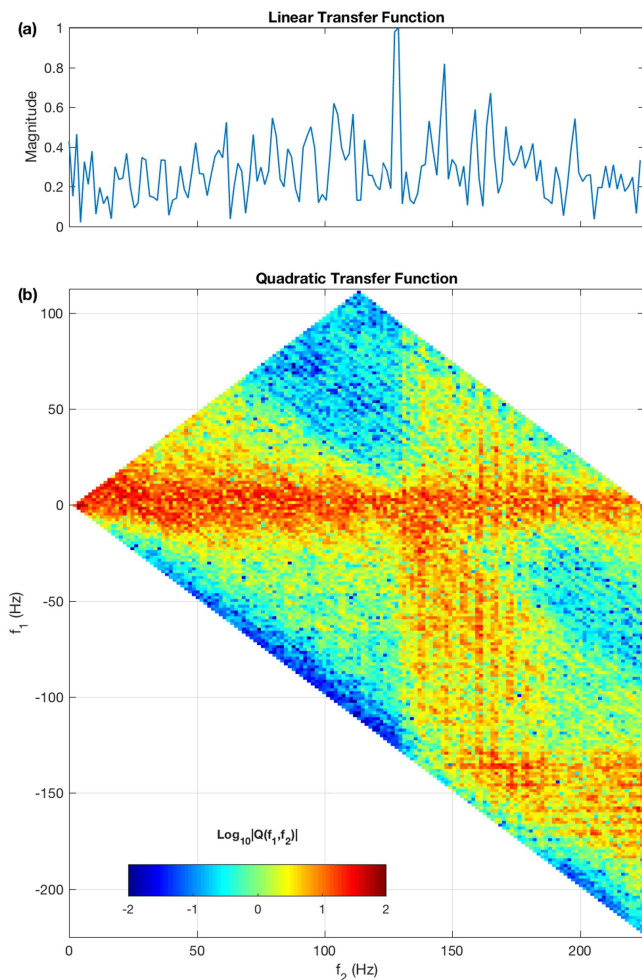


**Figure 3.** Results of the transfer function analysis for the period 184015–184025. Panel a shows the linear transfer function. Panel b shows quadratic transfer function for the frequency combinations  $f_1 + f_2 = f_3$  (region  $f_1 > 0$ ) and  $f_1 - f_2 = f_3$  (region  $f_1 < 0$ ).

order of 0.02–0.04 nT at frequencies below those of interest. At the frequencies of interest, that is, the frequency range in which the harmonics are observed, the amplitudes are around 2–3 pT. A comparison of the waveforms shows that there is some similarity between the two sets of measurements with features observed on Cluster 4 typically 0.15 s before Cluster 3. Thus, for the purposes of the transfer function estimation the measurements from Cluster 4 may be considered as the input, and Cluster 3 the output.

Figures 2b and 2c show the wavelet spectrograms of the Cluster 3 and 4 waveforms. These panels show typically  $\sim 10$  bands of EMW occurring in the frequency range 130–180 Hz. The resolution of the individual wave frequencies also implies that the scales/frequencies used in the wavelet transform are sufficient to resolve the waves of interest. The amplitude of the waves at a particular frequency is not constant, varying by up to 2 orders of magnitude between limits of approximately  $1 \times 10^{-7}$  and  $5 \times 10^{-6}$  nT<sup>2</sup>/Hz, independently for each of the observed proton gyrofrequency harmonics.

### 3.1. Transfer Function

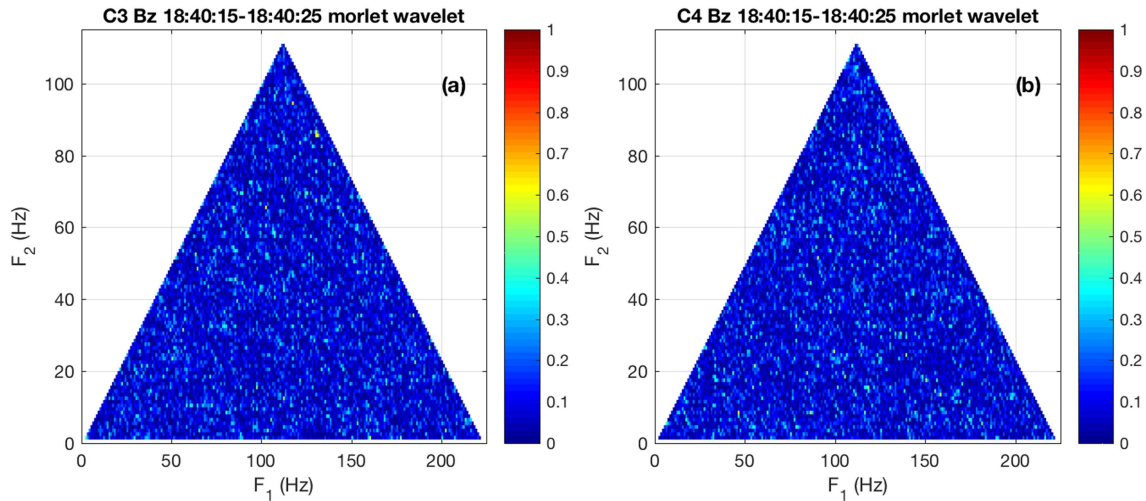
As mentioned previously, from the comparison of the waveforms it appears that Cluster 4 sees changes in the signal slightly before Cluster 3. Therefore, for the purposes of this study, the signal from Cluster 4 was taken as the input signal, Cluster 3 the output. In the original methodology of Ritz and Powers (1986) a Fourier Transform was used to transfer the signal from the time to the frequency domain. The transfer function (6) was then solved using an iterative scheme, beginning by estimating the value of the linear transfer function, using it to calculate the quadratic transfer function, followed by reestimating the linear transfer function coefficient and so on until the changes in the linear/quadratic transfer function coefficients is less than a predefined threshold level. The solution was later improved (Kim & Powers, 1988; Nam & Powers, 1994) by expanding (6) into a system of linear equations, rewriting them in matrix form using a method similar to a least squares fit for their solution. A similar least squares fit solution was also used by Dudok de Wit et al. (1999) and McCaffrey et al. (2000) for studies of turbulence at the terrestrial bow shock. These latter studies also employed a continuous wavelet transform to transform the data into the frequency domain. The solution methodology used in this study has previously been used in studies of shock turbulence (Giagkiozis et al., 2011).

Figure 3 shows the results of the transfer function calculations. Figure 3a shows the linear transfer function. Values below unity indicate the decay of waves from the input measurements to the output; values above unity indicate growth. Typical values for the frequency range being investigated are 0.6–0.8. This indicates that the waves are damped slightly as they propagate from Cluster 4 to 3.

Figure 3b shows the variations in the quadratic transfer function. The section above the frequency  $f_1 = 0$  represents interactions involving the summation of frequency components  $f_1$  and  $f_2$  where as below this line interactions are characterized by the difference of the frequency components. The results displayed indicate that the typical magnitude of the quadratic transfer function for waves in the frequency range 125–190 Hz is around  $10 \text{ nT}^{-1} \text{ Hz}^{1/2}$ . This would imply that three-wave interaction would generate wave amplitudes of the order  $5 \times 10^{-5}$  nT, a value that is negligible in comparison with the size of the measured signal. Therefore, the low values of the quadratic components of the transfer function indicate that there are no significant nonlinear interactions occurring within the system considered.

### 3.2. Bicoherence

To further investigate the significance of the role of wave-wave interactions in the growth/decay of the EMW observed, a bicoherence analysis was performed on the 10-s snapshot of data. As a tool for investigating the



**Figure 4.** Results of the bicoherence analysis for the period 18:40:15–18:40:25. Panels a and b show bicoherence results for Cluster 3 and 4, respectively.

occurrence of nonlinear interactions, bicoherence has previously been applied to waves in the front of the terrestrial bow shock (Walker et al., 1999; Wilson III et al., 2017), transmitter signals (Němec et al., 2017), and chorus waves (Gao et al., 2017). The bicoherence (normalized bispectrum), defined by (9), analyzes the phases of the triad of waves to determine the degree of correlation. Values of the order unity indicate strong correlation; zero indicates no correlation. A correlation of the phases implies a correlation between the wave numbers of the waves at frequencies  $\omega$ ,  $\omega_1$ , and  $\omega_2$ , so satisfying the resonance condition (3).

$$B(\omega_1, \omega_2) = \frac{|(X(\omega_1)X(\omega_2)X^*(\omega_1 + \omega_2))|^2}{(|X(\omega_1)X(\omega_2)|^2)|X^*(\omega_1 + \omega_2)|^2} \quad (9)$$

Figures 4a and 4b show the results of the bicoherence analysis using 10-s data snapshots from Cluster 3 and 4, respectively. The color scale represents values on the bicoherence in the range zero to unity. Examination of these plots shows that the bicoherence values are less than 0.1. This is interpreted as signifying that there is no correlation between the phases of the individual triads of waves analyzed and hence no correlation between the wave numbers of these waves. Thus, it appears that there are no nonlinear, three-wave interactions occurring within the data snapshot analyzed.

### 3.3. Other Periods

In total, eight 10-s snapshots centered on times between 18:40:15 and 18:47:45 UT were analyzed. Each snapshot showed very similar results to that presented above, namely, a transfer function whose quadratic interaction coefficients resulted in a negligible contribution to the overall waveform together with a bicoherence analysis that did not show any evidence for the occurrence of nonlinear, three-wave interactions.

## 4. Conclusions

This paper has presented the results of an analysis to determine the occurrence and role of nonlinear, three-wave interactions in the evolution of EMWs observed by the Cluster satellites. The main findings may be summarized as follows.

- Analysis of the blackbox transfer function, using Cluster 4 measurements as the input and Cluster 3 as output, showed that the quadratic terms within the transfer function resulted in a negligible contribution to the overall amplitude of the magnetic waveform.
- A bicoherence analysis yielded no evidence for the occurrence of nonlinear, three-wave interactions.

The analysis presented in this paper has shown no evidence for the occurrence of nonlinear interactions between the individual, discrete EMW emissions. These results lead to the conclusion that nonlinear interactions do not play a role in the generation and evolution of EMWs.

**Acknowledgments**

M. A. B. and H. A. acknowledge funding from STFC (Grant ST/R000697/1). The authors wish to thank the Cluster STAFF and FGM instrument teams for the provision of the data used in this study. All data used in this study were obtained from the Cluster Science Archive (<https://csa.esac.esa.int/csa-web/>).

**References**

Balikhin, M. A., Shprits, Y. Y., Walker, S. N., Chen, L., Cornilleau-Wehrin, N., Dandouras, I., et al. (2015). Observations of discrete harmonics emerging from equatorial noise. *Nature Communications*, *6*, 7703. <https://doi.org/10.1038/ncomms8703>

Balogh, A., Dunlop, M. W., Cowley, S. W. H., Southwood, D. J., Thomlinson, J. G., Glassmeier, K. H., et al. (1997). The Cluster magnetic field investigation. *Space Science Reviews*, *79*, 65–91. <https://doi.org/10.1023/A:1004970907748>

Billings, S. A. (2013). *Nonlinear systems identification: NARMAX, methods in the time, frequency, and spatio-temporal domains*. United Kingdom: Wiley-Blackwell.

Boardsen, S. A., Gallagher, D. L., Gurnett, D. A., Peterson, W. K., & Green, J. L. (1992). Funnel-shaped, low-frequency equatorial waves. *Journal of Geophysical Research*, *97*, 14967. <https://doi.org/10.1029/92JA00827>

Boardsen, S. A., Hospodarsky, G. B., Kletzing, C. A., Engebretson, M. J., Pfaff, R. F., Wygant, J. R., et al. (2016). Survey of the frequency dependent latitudinal distribution of the fast magnetosonic wave mode from Van Allen Probes Electric and Magnetic Field Instrument and Integrated Science waveform receiver plasma wave analysis. *Journal of Geophysical Research: Space Physics*, *121*, 2902–2921. <https://doi.org/10.1002/2015JA021844>

Boardsen, S. A., Hospodarsky, G. B., Kletzing, C. A., Pfaff, R. F., Kurth, W. S., Wygant, J. R., & MacDonald, E. A. (2014). Van allen probe observations of periodic rising frequencies of the fast magnetosonic mode. *Geophysical Research Letters*, *41*, 8161–8168. <https://doi.org/10.1002/2014GL062020>

Cornilleau-Wehrin, N., Chauveau, P., Louis, S., Meyer, A., Nappa, J. M., Perraut, S., et al. the STAFF Investigator Team (1997). The Cluster Spatio-Temporal Analysis of Field Fluctuations (STAFF) experiment. *Space Science Reviews*, *79*, 107–136. <https://doi.org/10.1023/A:1004979209565>

Dudok de Wit, T., Krasnoselskikh, V. V., Dunlop, M., & Lühr, H. (1999). Identifying nonlinear wave interactions in plasmas using two-point measurements: A case study of short large amplitude magnetic structures (SLAMS). *Journal of Geophysical Research*, *104*, 17,079–17,090. <https://doi.org/10.1029/1999JA900134>

Escoubet, C. P., Schmidt, R., & Goldstein, M. L. (1997). Cluster—Science and mission overview. *Space Science Reviews*, *79*, 11–32. <https://doi.org/10.1023/A:1004923124586>

Fu, H. S., Cao, J. B., Zhima, Z., Khotyaintsev, Y. V., Angelopoulos, V., Santolik, O., et al. (2014). First observation of rising-tone magnetosonic waves. *Geophysical Research Letters*, *41*, 7419–7426. <https://doi.org/10.1002/2014GL061687>

Gao, X., Lu, Q., & Wang, S. (2017). First report of resonant interactions between whistler mode waves in the Earth’s magnetosphere. *Geophysical Research Letters*, *44*, 5269–5275. <https://doi.org/10.1002/2017GL073829>

Gao, X., Sun, J., Lu, Q., Chen, L., & Wang, S. (2018). Generation of lower harmonic magnetosonic waves through nonlinear wave-wave interactions. *Geophysical Research Letters*, *45*, 8029–8034. <https://doi.org/10.1029/2018GL079090>

Giagkiozis, I., Walker, S. N., & Balikhin, M. A. (2011). Dynamics of ion sound waves in the front of the terrestrial bow shock. *Annales Geophysicae*, *29*(5), 805–811. <https://doi.org/10.5194/angeo-29-805-2011>

Gurnett, D. A. (1976). Plasma wave interactions with energetic ions near the magnetic equator. *Journal of Geophysical Research*, *81*, 2765–2770. <https://doi.org/10.1029/JA081i016p02765>

Horne, R. B., Thorne, R. M., Glauert, S. A., Meredith, N. P., Pokhotelov, D., & Santolik, O. (2007). Electron acceleration in the Van Allen radiation belts by fast magnetosonic waves. *Geophysical Research Letters*, *34*, L17107. <https://doi.org/10.1029/2007GL030267>

Horne, R. B., Wheeler, G. V., & Alleyne, H. S. C. K. (2000). Proton and electron heating by radially propagating fast magnetosonic waves. *Journal of Geophysical Research*, *105*, 27,597–27,610. <https://doi.org/10.1029/2000JA000018>

Kim, K. I., & Powers, E. J. (1988). A digital method of modeling quadratically nonlinear systems with a general random input. *IEEE Transactions on Acoustics Speech and Signal Processing*, *36*, 1758–1769. <https://doi.org/10.1109/29.9013>

Laakso, H., Junginger, H., Schmidt, R., Roux, A., & de Villedary, C. (1990). Magnetosonic waves above fc(H+) at geostationary orbit—GEOS 2 results. *Journal of Geophysical Research*, *95*, 10,609–10,621. <https://doi.org/10.1029/JA095IA07p10609>

Lyons, L. R., & Williams, D. J. (1984). *Quantitative aspects of magnetospheric physics*. Dordrecht, Holland: D. Reidel.

McCaffrey, D., Bates, I., Balikhin, M. A., Alleyne, H. S. C. K., Dunlop, M., & Baumjohann, W. (2000). Experimental method for identification of dispersive three-wave coupling in space plasma. *Advances in Space Research*, *25*(7/8), 1571–1577. [https://doi.org/10.1016/S0273-1177\(99\)00670-5](https://doi.org/10.1016/S0273-1177(99)00670-5)

McClements, K. G. (1996). Ion cyclotron harmonic waves in the equatorial magnetosphere. *Advances in Space Research*, *17*, 73–81.

Meredith, N. P., Horne, R. B., & Anderson, R. R. (2008). Survey of magnetosonic waves and proton ring distributions in the Earth’s inner magnetosphere. *Journal of Geophysical Research*, *113*, 6213. <https://doi.org/10.1029/2007JA012975>

Min, K., & Liu, K. (2016). Understanding the growth rate patterns of ion Bernstein instabilities driven by ring-like proton velocity distributions. *Journal of Geophysical Research: Space Physics*, *121*, 3036–3049. <https://doi.org/10.1002/2016JA022524>

Němec, F., Santolik, O., Hrbáčková, Z., Pickett, J. S., & Cornilleau-Wehrin, N. (2015). Equatorial noise emissions with quasiperiodic modulation of wave intensity. *Journal of Geophysical Research: Space Physics*, *120*, 2649–2661. <https://doi.org/10.1002/2014JA020816>

Němec, F., Čížek, K., Parrot, M., Santolik, O., & Záhlava, J. (2017). Line radiation events induced by very low frequency transmitters observed by the DEMETER spacecraft. *Journal of Geophysical Research: Space Physics*, *122*, 7226–7239. <https://doi.org/10.1002/2017JA024007>

Nam, S. W., & Powers, E. J. (1994). Application of higher order spectral analysis to cubically nonlinear system identification. *IEEE Transactions on Signal Processing*, *42*, 1746–1765. <https://doi.org/10.1109/78.298282>

Perraut, S., Roux, A., Robert, P., Gendrin, R., Sauvaud, J. A., Bosqued, J. M., et al. (1982). A systematic study of ULF waves above F<sub>H+</sub> from GEOS 1 and 2 measurements and their relationship with proton ring distributions. *Journal of Geophysical Research*, *87*, 6219.

Posch, J. L., Engebretson, M. J., Olson, C. N., Thaller, S. A., Breneman, A. W., Wygant, J. R., et al. (2015). Low-harmonic magnetosonic waves observed by the Van Allen Probes. *Journal of Geophysical Research: Space Physics*, *120*, 6230–6257. <https://doi.org/10.1002/2015JA021179>

Ritz, C. P., & Powers, E. J. (1986). Estimation of nonlinear transfer functions for fully developed turbulence. *Physica Scripta*, *20D*, 320. [https://doi.org/10.1016/0167-2789\(86\)90036-9](https://doi.org/10.1016/0167-2789(86)90036-9)

Russell, C. T., Holzer, R. E., & Smith, E. J. (1970). OGO 3 observations of ELF noise in the magnetosphere: 2. The nature of the equatorial noise. *Journal of Geophysical Research*, *75*, 755. <https://doi.org/10.1029/JA075i004p00755>

Sagdeev, R. Z., & Galeev, A. A. (1969). *Nonlinear plasma theory*.

Santolik, O., Parrot, M., & Němec, F. (2016). Propagation of equatorial noise to low altitudes: Decoupling from the magnetosonic mode. *Geophysical Research Letters*, *43*, 6694–6704. <https://doi.org/10.1002/2016GL069582>

Shklyar, D. R., & Balikhin, M. A. (2017). Whistler mode waves below lower hybrid resonance frequency: Generation and spectral features. *Journal of Geophysical Research: Space Physics*, *122*, 10,072–10,083. <https://doi.org/10.1002/2017JA024416>

- Sun, J., Gao, X., Chen, L., Lu, Q., Tao, X., & Wang, S. (2016). A parametric study for the generation of ion Bernstein modes from a discrete spectrum to a continuous one in the inner magnetosphere. I. Linear theory. *Physics of Plasmas*, 23(2), 022901. <https://doi.org/10.1063/1.4941283>
- Sun, J., Gao, X., Lu, Q., Chen, L., Tao, X., & Wang, S. (2016). A parametric study for the generation of ion Bernstein modes from a discrete spectrum to a continuous one in the inner magnetosphere. II. Particle-in-cell simulations. *Physics of Plasmas*, 23(2), 022902. <https://doi.org/10.1063/1.4941284>
- Tsurutani, B. T., Falkowski, B. J., Pickett, J. S., Verkhoglyadova, O. P., Santolik, O., & Lakhina, G. S. (2014). Extremely intense ELF magnetosonic waves: A survey of polar observations. *Journal of Geophysical Research: Space Physics*, 119, 964–977. <https://doi.org/10.1002/2013JA019284>
- Walker, S. N., Balikhin, M. A., & Nozdrachev, M. N. (1999). Ramp nonstationarity and the generation of whistler waves upstream of a strong quasiperpendicular shock. *Geophysical Research Letters*, 26(10), 1357–1360. <https://doi.org/10.1029/1999GL900210>
- Wilson III, L. B., Koval, A., Szabo, A., Stevens, M. L., Kasper, J. C., Cattell, C. A., & Krasnoselskikh, V. V. (2017). Revisiting the structure of low-Mach number, low-beta, quasi-perpendicular shocks. *Journal of Geophysical Research: Space Physics*, 122, 9115–9133. <https://doi.org/10.1002/2017JA024352>
- Zhima, Z., Chen, L., Fu, H., Cao, J., Horne, R. B., & Reeves, G. (2015). Observations of discrete magnetosonic waves off the magnetic equator. *Geophysical Research Letters*, 42, 9694–9701. <https://doi.org/10.1002/2015GL066255>